Ocean Dynamics (2018) 68:1259–1272
https://doi.org/10.1007/s10236-018-1193-1

On the interaction between a hurricane, the Gulf Stream and coastal sea level

Tal Ezer[1]

Received: 9 April 2018 / Accepted: 29 June 2018 / Published online: 7 July 2018

Abstract

Tropical storms and hurricanes in the western North Atlantic Ocean can impact the US East Coast in several ways. Direct effects include storm surges, winds, waves, and precipitation and indirect effects include changes in ocean dynamics that consequently impact the coast. Hurricane Matthew [October, 2016] was chosen as a case study to demonstrate the interaction between an offshore storm, the Gulf Stream (GS) and coastal sea level. A regional numerical ocean model was used, to conduct sensitivity experiments with different surface forcing, using wind and heat flux data from an operational hurricane-ocean coupled forecast system. An additional experiment used the observed Florida Current (FC) transport during the hurricane as an inflow boundary condition. The experiments show that the hurricane caused a disruption in the GS flow that resulted in large spatial variations in temperatures with cooling of up to ~ 4 °C by surface heat loss, but the interaction of the winds with the GS flow also caused some local warming near fronts and eddies (relative to simulations without a hurricane). A considerable weakening of the FC transport (~ 30%) has been observed during the hurricane (a reduction of ~ 10 Sv in 3 days; $1\mathrm{Sv} = 10^6\ \mathrm{m}^3\ \mathrm{s}^{-1}$), so the impact of the FC was explored by the model. Unlike the abrupt and large wind-driven storm surge (up to 2 m water level change within 12 h in the South Atlantic Bight), the impact of the weakening GS on sea level is smaller but lasted for several days after the hurricane dissipated, as seen in both the model and altimeter data. These results can explain observations that show minor tidal flooding along long stretches of coasts for several days following passages of hurricanes. Further analysis showed the short-term impact of the hurricane winds on kinetic energy versus the long-term impact of the hurricane-induced mixing on potential energy, whereas several days are needed to reestablish the stratification and rebuild the strength of the GS to its pre-hurricane conditions. Understanding the interaction between storms, the Gulf Stream and coastal sea level can help to improve prediction of sea level rise and coastal flooding.

Keywords Coastal sea level · Hurricanes · Flooding · Gulf stream · Florida current

1 Introduction

The two-way interaction between the ocean and tropical storms or hurricanes is usually centered on the heat exchange between the storm and surface ocean temperatures; this exchange is important for the storm's intensity and for ocean cooling (Bender and Ginis 2000; Shay et al. 2000; Li et al. 2002; Oey et al. 2006, 2007; Yablonski et al. 2015). Storms passing over the ocean can also cause increased mixing and changes in ocean currents, as seen for example during Hurricane Wilma [2005], which affected the flow of the Loop Current in the Gulf of Mexico (Oey et al. 2006). Hurricanes and tropical storms often move across the southwestern North Atlantic, where the dominant current is the Gulf Stream (GS). Several studies thus suggest that storms in this area can cause a temporary (but large) reduction in the GS transport. Evidences of such impact of hurricanes on the GS were reported for example, for Hurricane Bill (2009) (Kourafalou et al. 2016), Hurricane Joaquin [2015] (Ezer and Atkinson 2017; Ezer 2018), and Hurricane Mathew [2016] (Ezer et al. 2017). Comparisons of the time when hurricanes and tropical storms passed the southwestern North Atlantic over the last three decades with the observed transport of the Florida Current (FC) suggest that these seasonal storms can even influence the seasonal cycle of the FC (Ezer 2018). Note that interactions between Pacific Ocean Typhoons and the Kuroshio Current have also been studied in a similar manner (Wu et al. 2008; Liu and Wei 2015).

There are four main mechanisms in which intense storms can impact the GS. First, Atlantic tropical storms spend

Responsible Editor: Dirk Olbers

✉ Tal Ezer
tezer@odu.edu

1 Center for Coastal Physical Oceanography, Old Dominion University, 4111 Monarch Way, Norfolk, VA 23508, USA

considerable time south or east of the GS before either turning northwest and making landfall on the US East Coast (e.g., Hurricane Sandy, 2012) or moving back offshore (e.g., Hurricane Joaquin, 2015, and Hurricane Matthew, 2016). During this time, the counterclockwise wind is blowing against the northeastward clockwise flow of the GS and can significantly interrupt the GS flow (Ezer et al. 2017; Ezer 2018). Second, the surface heat loss from the upper ocean (Bender and Ginis 2000; Shay et al. 2000) which empower the hurricane can cool down the warm GS and the supply of warm waters into higher latitudes downstream. Third, the intense vertical mixing induced by the strong winds and large waves under the hurricane can degrade the sharp horizontal thermal gradients across the GS; this pressure gradient is the baroclinic geostrophic part of the GS flow. Fourth, the storm surge can pileup water on the coast (on the onshore side of the GS), reducing the sea surface height difference between the onshore and offshore sides of the GS; this will lead to a reduction in the barotropic geostrophic part of the GS flow. The above mechanisms are not independent of each other and can combine to contribute to the reduction of the GS flow (but potentially also to increase flow at some locations if the wind-driven current is in the GS flow direction). These mechanisms were recently studied by Ezer et al. (2017), analyzing output from a NOAA's operational coupled hurricane-ocean modeling system during Hurricane Matthew. However, the operational forecast system, running in real time during a hurricane, does not allow assessment of various aspects of the air-sea coupled system. For example, it is not clear how much of the sea surface temperature change during the hurricane was due to heat loss or due to mixing. Another limitation of using an operational modeling system was that the ocean model part of the coupled system was a basin-scale ocean model that was not intended to be a storm surge prediction model (though it did a decent job in its coastal sea level simulation; Ezer et al. 2017). Therefore, in the present study, the momentum and heat fluxes from the coupled system are used to force a regional coastal ocean model (see domain in Fig. 1), and various sensitivity experiments were performed with different forcing, which was not possible with the real-time forecast system.

Another aspect of the study is the potential remote influence of a storm on coastal sea level along the US East Coast through the impact of the storm on the flow and structure of the GS. As reported in recent studies, a weakening in the GS flow is often associated with a decrease in the sea level slope across the GS and elevated coastal sea level on the onshore side of the current (Ezer et al. 2013; Ezer and Atkinson 2014, 2017; Ezer 2015, 2016; Ezer et al. 2017; Goddard et al. 2015; Park and Sweet 2015; Wdowinski et al. 2016). This relation between variations in the GS and coastal sea level had been suggested long time ago (Blaha 1984), but this connection received more attention in recent years since rising sea levels brought many places over a threshold when even a small anomaly over the predicted tide can now cause minor flooding (Ezer and Atkinson 2014). The GS-coastal sea level connection can be detected on a wide range of scales, from long-term sea level acceleration (Boon 2012; Ezer and Corlett 2012; Sallenger et al. 2012) due to potential slowdown of the Atlantic Meridional Overturning Circulation (AMOC) (McCarthy et al. 2012; Smeed et al. 2013) to short-term daily fluctuations (Ezer 2016). The present study focuses on short-term variability associated with the interaction of the GS with a hurricane. Due to sea level rise, many coastal cities such as Norfolk, VA, or Miami, FL, have seen acceleration in minor flooding, so that even a slightly elevated water level due to short-term variations in the GS can now cause unexpected tidal flooding (so called "clear day" or "nuisance" flooding) even when there is no storm nearby (Ezer and Atkinson 2014; Park and Sweet 2015; Wdowinski et al. 2016). The mechanism of this observed short-term sea level-GS correlation was explored by Ezer (2016), who showed the role of fast moving barotropic signals that generate coastal trapped waves. The roles of changing wind patterns and atmospheric pressure in coastal sea level variability are also important (Piecuch and Ponte 2015; Piecuch et al. 2016; Woodworth et al. 2016), but they will not be discussed here.

The case study presented here involves Hurricane Matthew which developed in the Caribbean in late September 2016, and then moved northward along the southeastern US coast in October 7–9 (Fig. 2), causing significant flood damage due to rain and storm surge on coasts from the South Atlantic Bight (SAB) to the Mid-Atlantic Bight (MAB). This hurricane did not make landfall, but it stayed for several days near the GS, causing as much as 50% temporary reduction in its flow, as evident in various observations and models (Ezer et al. 2017). Therefore, this is a good case study to demonstrate the interaction between a hurricane and ocean currents. The main goal of the study is to investigate under controlled model experiments the various interactions between the hurricane, the GS, and coastal sea level, so that better understanding of the mechanisms involved is obtained.

The study is organized as follows. First, the data sources and the model setting are described in Sect. 2, then results of the different experiments are presented in Sect. 3, and finally a summery and conclusions are offered in Sect. 4.

2 Data and model experiments

Six tide gauge stations, three in the SAB and three in the MAB, are used here (Fig. 1); hourly water levels were obtained from NOAA (http://opendap.co-ops.nos.noaa.gov/dods/). Measurements of the daily FC transport by the cable across the Florida Strait (at ~27°N) started in 1982 (Baringer and Larsen 2001; Meinen et al. 2010) and available from NOAA's Atlantic Oceanographic and Meteorological Laboratory web page (www.aoml.noaa.gov/phod/

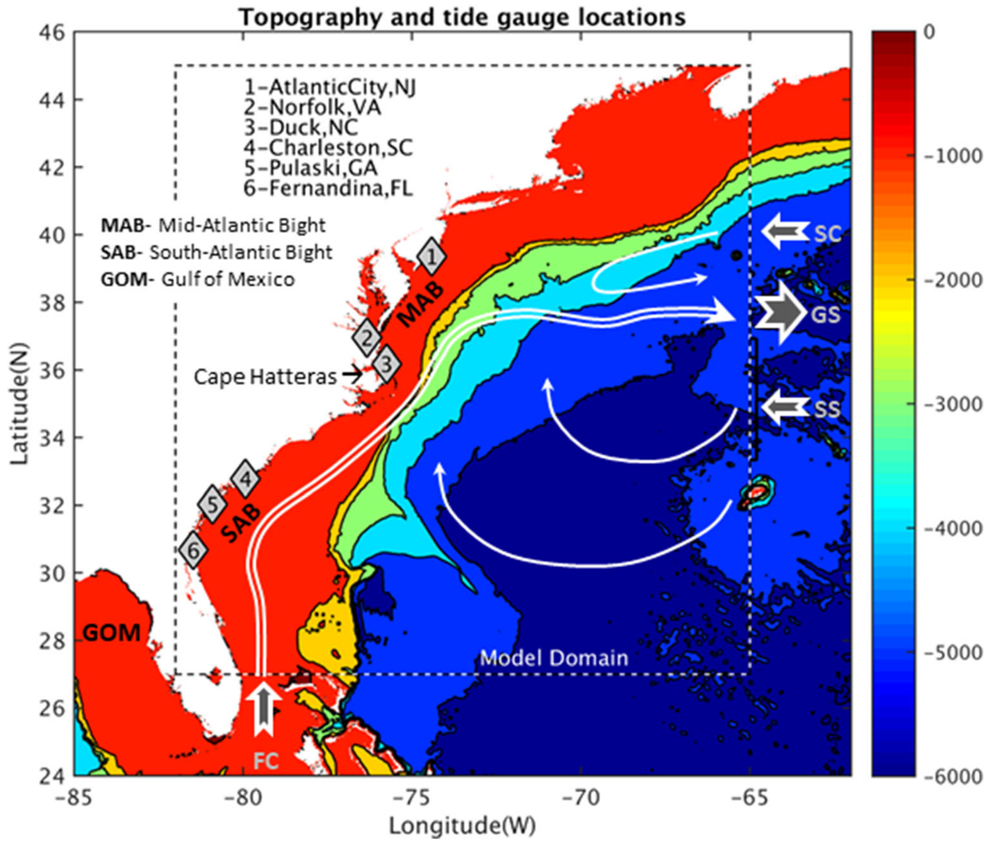

Fig. 1 Bottom topography (color in meter) of the region and model domain (dashed line). Six tide gauge stations used in the study are indicated (diamonds with numbers). The location of imposed model's inflows (Florida Current, FC; Slope Current, SC and Sargasso Sea, SS) and outflow (Gulf Stream, GS) are indicated (wide arrows), as well as schematic of the main currents (narrow arrows)

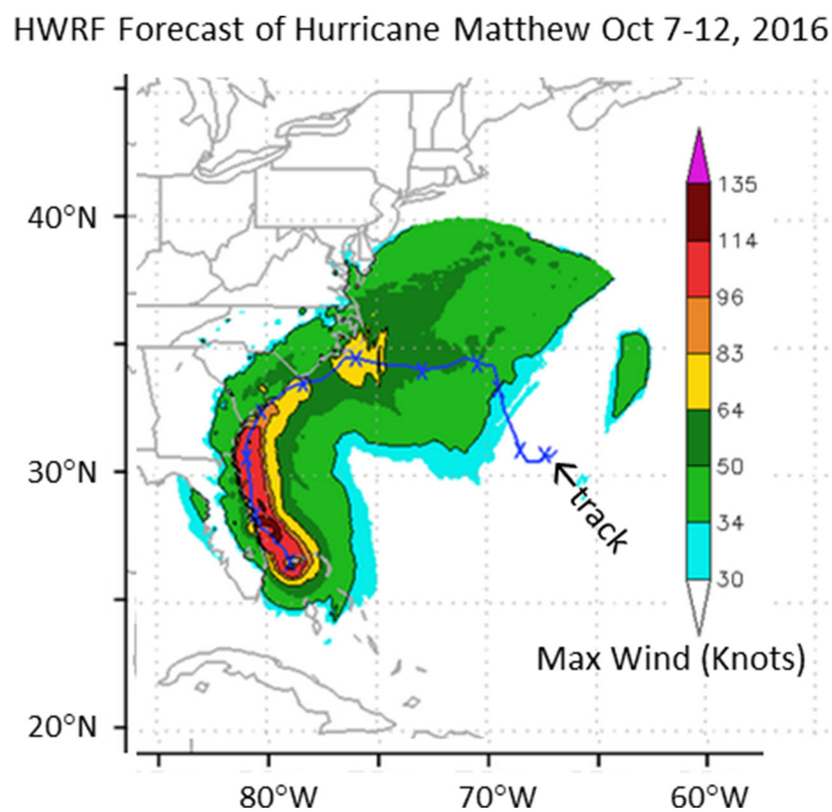

Fig. 2 The maximum wind field (color in knots) from the operational forecast of the HWRF-POM model for Hurricane Matthew (October 7–12, 2016) and storm predicted track ("x" and blue line). The figure is a modified version of the one on the NOAA site (http://www.emc.ncep.noaa.gov/gc_wmb/vxt/HWRF/)

floridacurrent/); here, only the data for October, 2016, were used. Six-hourly output from NOAA's coupled operational Hurricane Weather Research and Forecasting (HWRF) and the Princeton Ocean Model (POM) (Yablonsky et al. 2015; Tallapragada et al. 2014) were obtained for the period October 7–12, 2016, when the operational system simulated Hurricane Matthew. The same coupled model for the same period had been recently analyzed (see Ezer et al. 2017, for details). The model domain covers the western North Atlantic Ocean (10°N–47.5°N, 30°W–100°W). Here, data for only a smaller sub-region were used (Fig. 1), whereas six-hourly fields of surface heat flux and surface wind stress from the coupled model were used as surface boundary conditions of a regional ocean model.

The regional ocean model used here (see domain in Fig. 1) is the same as used recently for coastal sea level studies (see Ezer 2016 and Ezer 2017, for details). The numerical ocean model code is based on the generalized coordinate model of Mellor et al. (2002) with a terrain-following vertical grid and a Mellor-Yamada turbulence scheme. The model topography was obtained from the ETOPO5 data with minimum depth of 10 m. The horizontal grid is cartesian with 1/12° resolution (~ 6–8 km grid size), and the vertical grid is sigma (terrain-following) with 21 layers (higher resolution near the surface). The initial condition is the monthly temperature and salinity data. A spin up of 3 months seems to be sufficient for this small domain to produce a relatively realistic-looking GS (Ezer 2016, 2017). The experiments presented here started after the spin up and represent simulations for October 1–15, 2016; in some experiments (see below), data for Hurricane Matthew was provided as forcing for October 7–12. Note, however, that without data assimilation and without much longer realistic forcing (surface and lateral boundary conditions), the simulations cannot represent realistic synoptic fields; thus, temperature, salinity, and the GS eddies and meanders represent natural variability, not the observed values in space and time at that period. This limitation is not of concern here, since the main purpose of the study is the comparison between different sensitivity experiments, not comparison of the model with observations. The only meaningful model-data comparison is for coastal sea level driven by the hurricane winds (see later). Five sensitivity experiments have been conducted:

1. Control case ("No Hurricane" experiment)—surface heat flux and surface wind stress are zero. The only forcing is a fixed imposed boundary transports (see Fig. 1): 30 Sv inflow of the Florida Current (FC), 40 Sv inflow of the Slope Current (SC), 30 Sv inflow of the Sargasso Sea (SS), and 100 Sv outflow of the Gulf Stream (GS). Only the total transport (vertically integrated velocity) is specified on the boundary together with standard barotropic radiation boundary conditions. The vertical distribution of the velocity near the open boundaries is calculated by the model from the density field in a 1° buffer zone near the southern and eastern open boundaries.
2. Hurricane wind case ("Wind" experiment)—surface wind stress from the coupled HWRF model is added for October 7–12 (during Hurricane Matthew). The wind is interpolated in space and time from the 6-hourly HWRF output into the ocean model. A smoothed transition is implemented at the beginning and end of the hurricane period. Note that in this case, surface heat flux is zero and inflow FC transport is constant as in experiment 1.
3. Hurricane heat flux case ("HF" experiment)—surface heat flux from the 6-hourly coupled HWRF model output is used for October 7–12. In this case, wind remains zero everywhere, so that heat loss during the hurricane can be separated from the wind effects. FC transport is constant as in experiment 1.
4. Full hurricane case ("Wind+HF" experiment)—both wind stress and heat flux from the HWRF output are used for October 7–12. FC transport remains constant as in experiment 1.
5. Florida Current case ("FC" experiment)—same as the control run (no wind and no heat flux), except that the constant inflow of the FC is replaced by the observed FC transport for October 1–15. The change in the inflow at the southern boundary at 27°N is balanced by similar outflow that allows to exit the model on the eastern boundary at 60°W, so volume is generally conserved. This experiment is like the experiments conducted by Ezer (2016), though in the latter study artificial oscillations in the FC transport was imposed, while here observed values are used.

Comparisons between experiments 2–4 and experiment 1 will demonstrate the impact of the hurricane wind versus the impact of the hurricane-driven oceanic heat loss, and comparisons between experiments 5 and 1 will show the impact of the FC. In the analysis, the impact of each forcing will be defined as the difference between a forced case and the control run. One should keep in mind, however, that in the real ocean, it is difficult to separate between the hurricane impact on the FC (when it passed very close to the Florida Strait) and the impact of the hurricane on the GS downstream when the hurricane moved north. In the model case, experiment 5 represents only the direct impact of the FC on the model (assuming that the hurricane impacts only the FC, but neglecting the wind impact on the rest of the GS) while experiment 4 represents the impact of the hurricane winds on the downstream GS (neglecting the change in the FC). Unlike the coupled HWRF-POM system, in the experiments conducted here there is no air-sea feedback.

3 Results

3.1 The impact of the hurricane and the Florida Current on coastal sea level

Storm surge models require high-resolution ocean models and accurate wind field at high temporal and spatial resolutions (e.g., see the storm surge model of the Chesapeake Bay in Garzon et al. 2017). The evaluation by Ezer et al. (2017) of the HWRF coupled model prediction during Hurricane Matthew shows some skill in the prediction of coastal sea level, though storm surge along the US East Coast was underestimated by ~30–50%. This deficiency was expected, since the ocean model part of the coupled system was intended to provide feedback to the hurricane prediction model but was not intended to be a storm surge model which requires more detailed coastal shoreline and topography (the 6-hourly HWRF output also limits the ability to compare the model with hourly tide gauge data).

The storm surge along the coast can be clearly seen in Fig. 3; it is defined as the difference (or anomaly) in sea level between experiment 4 and experiment 1. As the hurricane propagated northeastward along the coast, the onshore winds ahead of the storm piled up water on the coast (positive anomaly in red) while the offshore winds in the back of the storm pushed water away from the coast and sea level dropped (negative anomaly in blue). After day 10, the storm dissipated (no longer a hurricane) and

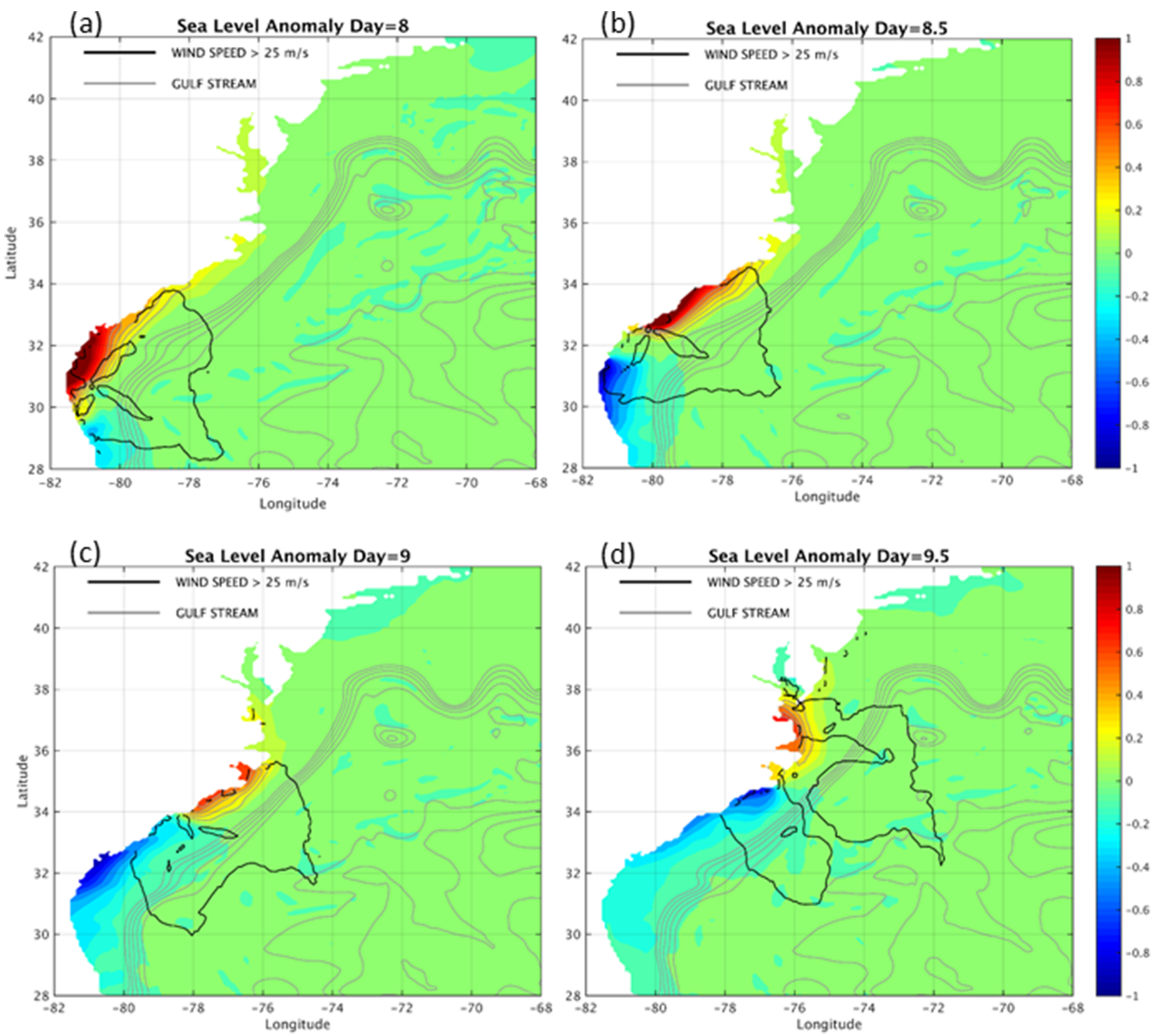

Fig. 3 The model storm surge (color in m) defined as the sea level difference (anomaly) between experiment 4 (WIND + HF) and experiment 1 (NO-HURRICANE); panels **a**–**d** are for days 8–9.5. The heavy black contours indicate the estimated extent of the strong winds (outer/inner lines are for wind speed > 25/35 m s^{-2}, respectively). The gray lines show a few contours of the absolute sea surface height in experiment 4, to indicate the location of the Gulf stream

moved offshore. However, after day 12, when the remains of the storm were more than 800 km from shore, the impact of the storm can still be seen as a higher than normal coastal sea level along the entire coast, from Florida to New Jersey, with particular high waters in the Chesapeake Bay (Fig. 4a). The fact that sea level north/south of the GS is higher/lower than normal indicates that the storm caused a reduction in the sea level slope across the GS and thus weakened the currents. Altimeter data of sea surface height anomaly (Fig. 4b) confirm the model results, showing higher than normal water along the northern edge of the GS and along the coast from Florida to New Jersey. Note that sea level anomaly is defined differently for the model (difference

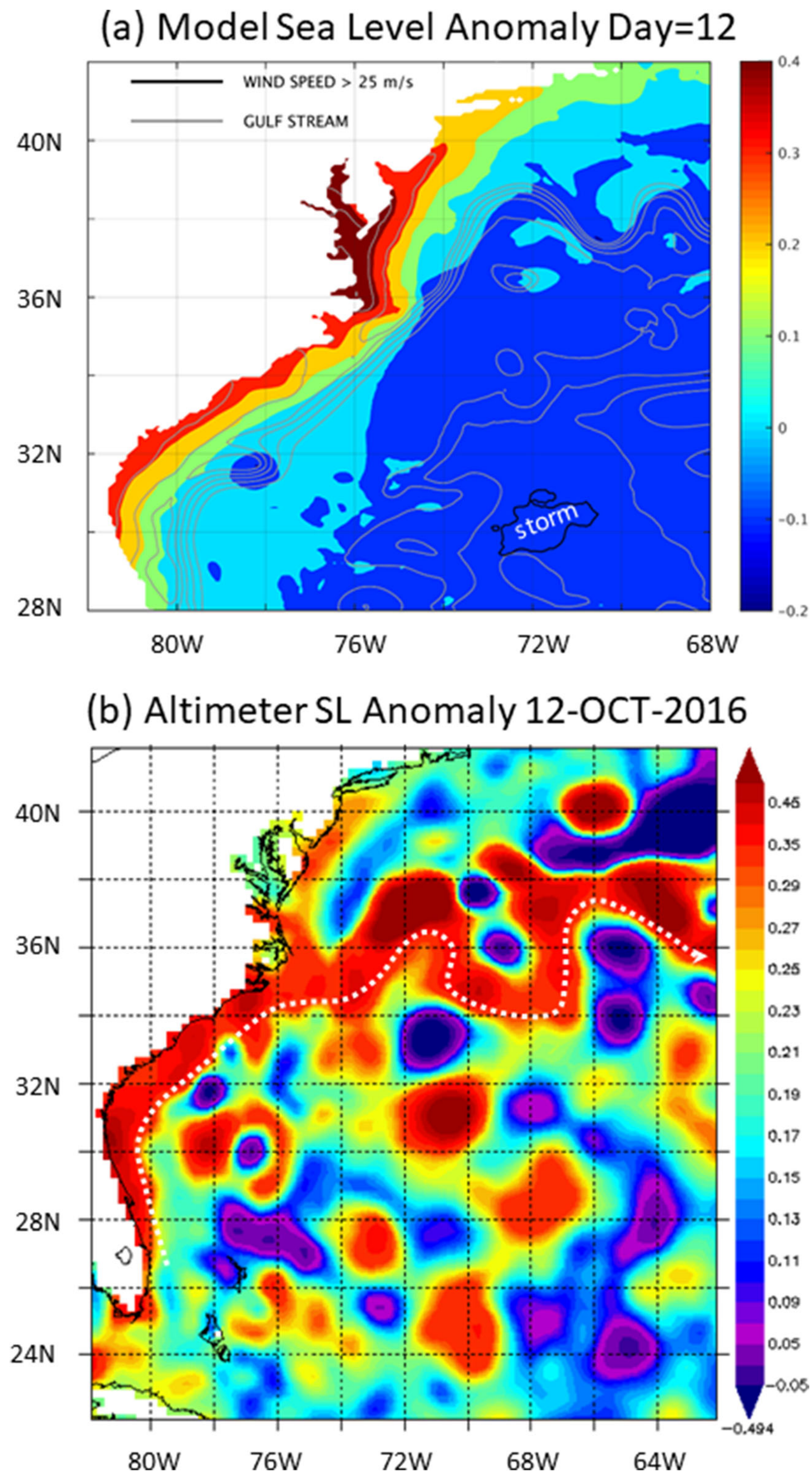

Fig. 4 **a** The model sea level anomaly as in Fig. 3, but for day 12 after the storm moved away from the coast (note that the color scale is different than that of Fig. 3). **b** Sea level anomaly from satellite altimeters (from AVISO) on October 12, 2016; the approximated location of the Gulf Stream is indicated by a dashed white line. Note that the domains and the color bars of **a** and **b** are different, and that sea level anomaly is defined differently: in **a**, the anomaly is the difference between two model simulations for the same day, while in **b**, the anomaly is the observed sea surface height at that day relative to a long-term mean of absolute sea surface height

between two model runs) and the altimeter data (anomaly relative to a long-term mean, which is not available in the model case); nevertheless, both model and satellite data agree on the main impact after the storm moved away. The results demonstrate the difference between a local short-term storm surge that moves with the storm (Fig. 3) and a longer-term, spatially wide impact due to ocean dynamics after the storm disappeared (Fig. 4).

Figure 5 shows a comparison of results from experiment 4 (Wind + HF) with hourly coastal sea level anomaly data. Note that the anomaly data (observed minus tidal prediction) provided by NOAA still had some tidal-like variations which may be related to resonant created by the hurricane. The range of coastal sea level variation during the storm, ~ 2 m between maximum storm surge and the water level decline in the wake of the storm, was simulated very well in the SAB (Fernandina, FL, Pulaski, GA, and Charleston, SC). A smaller storm surge of ~ 0.5–1 m was observed and simulated in the MAB (Duck, NC, Norfolk, VA, and Atlantic City, NJ). The skill of this model with respect to wind-driven coastal sea level is somewhat improved over the HWRF simulations (Ezer et al. 2017), though the same wind field was used. Note that observed water levels ahead of the storm were higher than normal due to previous weather systems (see Fig. 2a in Ezer et al. 2017), but the model only used wind data for October 7–12, so model-data comparisons outside this period are not expected to be very accurate. The observations in Fig. 5 show what looks like a quick recovery of sea level from the storm surge during the short period shown, but longer records (not shown) indicated that water level after the storm was higher than before along most of the SAB and MAB coasts—this can be seen in the altimeter data as well (Fig. 4b).

Analyzing various observations, including the FC transport, satellite altimeter data, and high-frequency radar data, Ezer et al. (2017) show evidence of significant

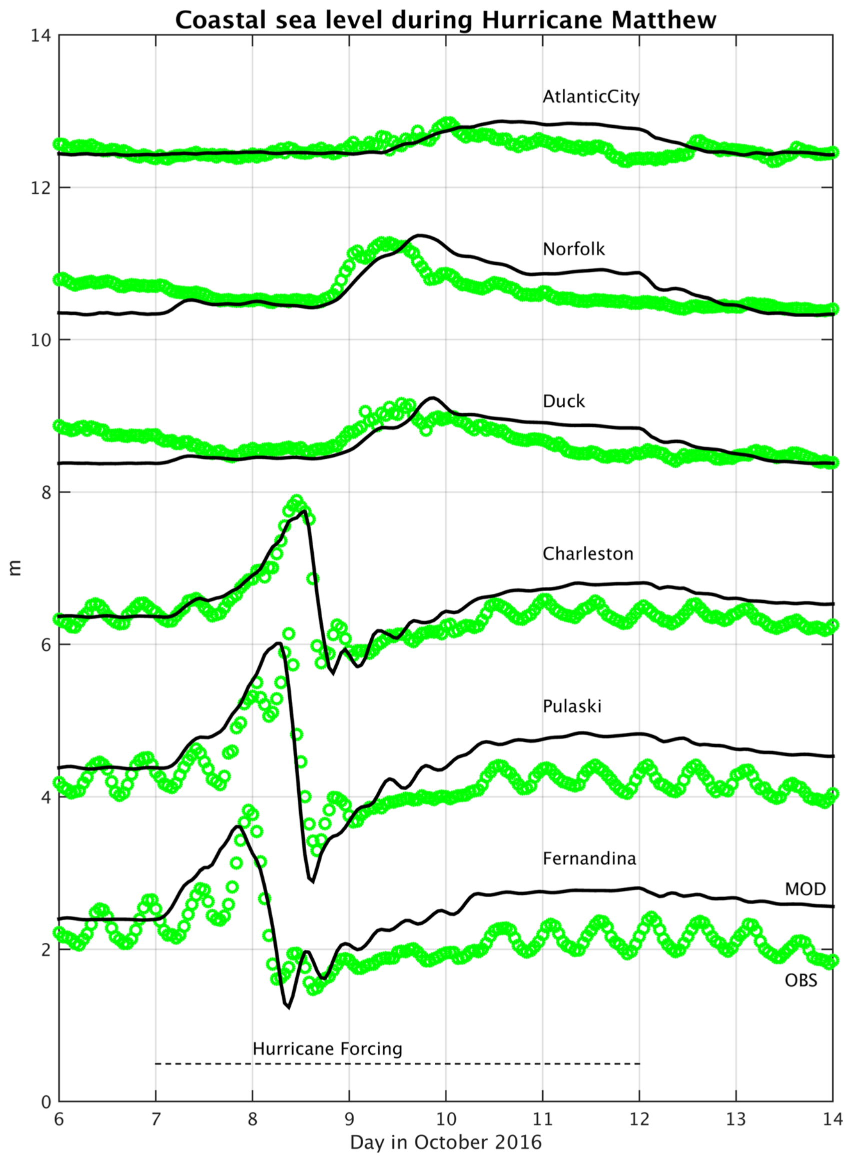

Fig. 5 Hourly water level anomalies at the six locations in Fig. 1 (relative values in m were vertically shifted for clarity) as obtained from the tide gauges (green circles; predicted tides were subtracted) and from the model forced by hurricane winds (experiment 4; black lines). Hurricane winds were applied in the model only during October 7–12 (dashed horizontal line)

decline in the GS flow during the passage of Hurricane Matthew (by as much as ~50% from the weeks before the hurricane). The observed FC transport at 27°N reflects part of this hurricane-driven change, so experiment 5 ("FC") was conducted to see the direct impact of the FC alone on coastal sea level, and the results are shown in Fig. 6. In 3 days, between October 8 and October 11, the FC transport weakened by ~30% (from ~30 to ~20 Sv; black heavy line in the bottom of Fig. 6). During these 3 days, water level at the 3 SAB stations rose by ~10 cm as a direct impact of the reduction in sea level slope across the GS. In the MAB (where the GS is farther away from the coast), sea level rose by a smaller amount (~2–5 cm). Note that in the experiments with the same model conducted by Ezer (2016, 2017), the coastal sea level response was similar in magnitude, but more coherent along the coast. However, the previous studies used a FC transport that oscillates at a constant frequency for a long period of time, which apparently allowed the ignition of coastal trapped waves along the coast, including resonant amplification at some critical frequencies (Ezer 2016). In any case, all these experiments indicate that in general, every 1 Sv decrease in the FC can cause ~1 cm increase in coastal sea level in the SAB. Observations of sea level in south Florida showed similar relation for long-term variations (Park and Sweet 2015). Sea level in the MAB is also anticorrelated with the GS transport (Ezer 2013, 2015, 2016; Ezer and Atkinson 2017), but the coastal response is more complex there because of the additional influence from variations in the Slope Current, shift in the GS path, and influence from GS meanders and eddies (Ezer et al. 2013).

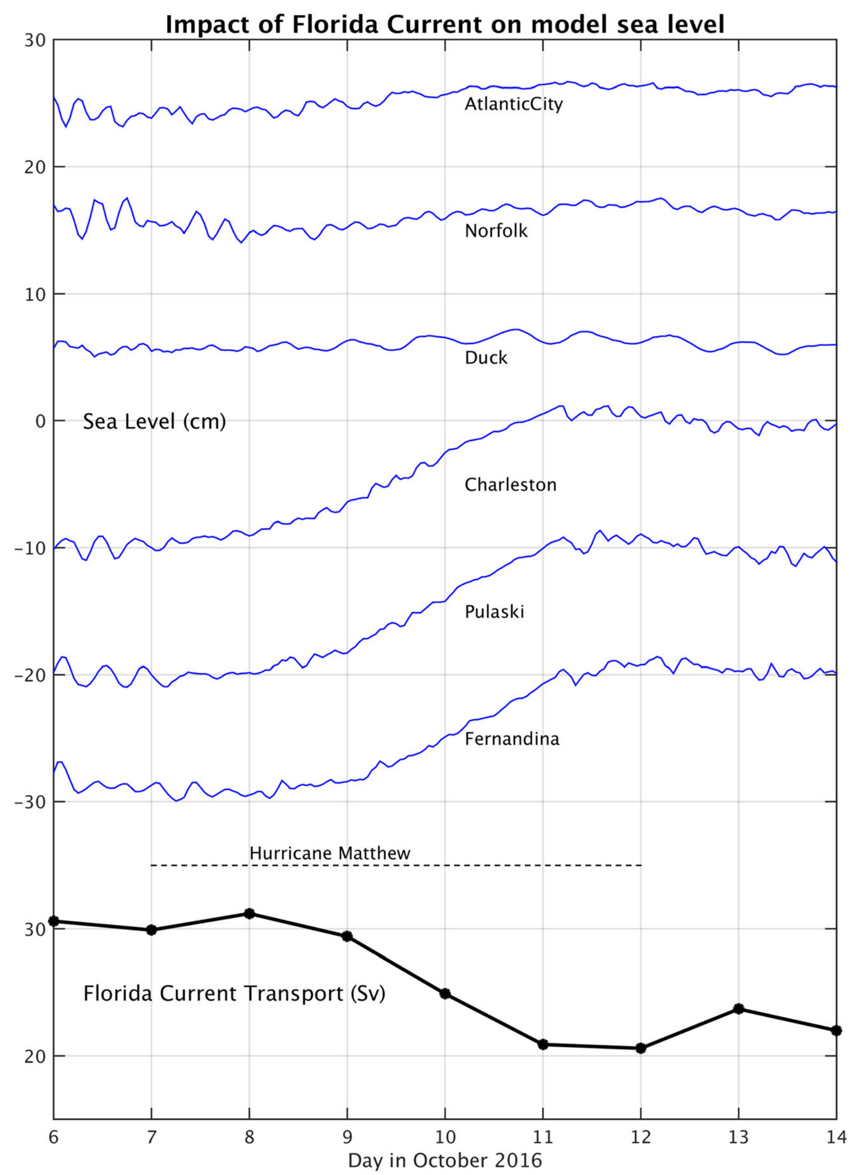

Fig. 6 Hourly simulated water levels (in cm, blue lines, shifted vertically for clarity) at the same locations as in Fig. 5, but without wind (experiment 5) when the only forcing of the model is the observed daily Florida Current transport (in Sv, black line at the bottom)

3.2 The impact of the hurricane on the Gulf Stream transport

As seen in Fig. 6, the FC transport at 27°N decreased by ~ 30% within 3 days, and as shown in Ezer et al. (2017), the GS flow when Hurricane Matthew dissipated may have been weaker by as much as ~ 50% from its flow a few weeks before Hurricane Matthew entered the region. The hurricane winds covered large portion of the model domain (Fig. 2) and thus can temporally affect the ocean circulation. To evaluate the impact of the hurricane on the circulation, the total stream function, ψ, is calculated from the vertically averaged velocity field, (U, V), integrated across the domain, starting from $\psi = 0$ on land (assuming surface elevation is smaller than water depth, $\eta \ll h$).

$$\psi(x,y,t) = -\iint_{x\,y} U(x,y,t)h(x,y)dy \quad \textbf{or} \quad \psi(x,y,t) = \iint_{x\,y} V(x,y,t)h(x,y)dx \tag{1a, b}$$

where

$$U(x,y,t) = \int_z u(x,y,z,t)dz \quad \textbf{and} \quad V(x,y,t) = \int_z v(x,y,z,t)dz \tag{2a, b}$$

so that

$$U = -\frac{\partial\psi}{\partial y} \quad , \quad V = \frac{\partial\psi}{\partial x} \quad \textbf{and} \quad \frac{\partial U}{\partial x} + \frac{\partial V}{\partial y} = 0 \tag{3a, b, c}$$

The stream function in experiment 4 is shown for 2 days, October, 8, 2016, when the hurricane was near the northern coast of Florida (Fig. 7a) and October 10, 2016, when the hurricane moved offshore off Cape Hatteras, North Carolina (Fig. 7b). When the hurricane was located close to the coast around 30°N, the generation of a clockwise circulation cell around the high value in red (Fig. 7c shows the difference between experiment 4 and experiment 1) could potentially increase the GS transport in the SAB by ~ 5 Sv ($\partial\psi/\partial x > 0$ in Eq. 3b). However, when the hurricane moved offshore around 35°N, an anticlockwise circulation cell around the low value in blue (Fig. 7d) was generated, forcing currents in the direction which potentially can reduce the GS transport by almost ~ 15 Sv. The impact on the circulation due to the FC transport alone (without wind) can be evaluated from the difference between experiment 5 ("FC") and experiment 1. When the inflow into the model was reduced, the GS transport was reduced by ~ 4 Sv on October 8 (Fig. 7e) and by ~ 10–15 Sv on October 10 (Fig. 7f). The combined impact of the winds and FC is in general agreement with the transport reduction shown in Ezer et al. (2017). Note that in the real ocean, the hurricane affects both the FC and the GS downstream, but in the model experiments, the two factors are separated to better understand the mechanism and pattern behind each impact and this is reflected in the differences between Fig. 7d, f.

3.3 The impact of the hurricane on surface temperatures and stratification

The impact of hurricanes on cooling of sea surface temperatures (SST) along the storm's path has been studied before (Bender and Ginis 2000; Shay et al. 2000; Li et al. 2002; Oey et al. 2006, 2007; Yablonski et al. 2015), but the mechanism may be more complex when the underlying ocean currents involve strong flows such as the GS. Figure 8 shows the SST and its changes when the hurricane started moving offshore and was located just off Cape Hatteras in October 10, 2016. Note that without long-term simulations with observed heat fluxes and data assimilation of the GS location and eddies, the model temperature in Fig. 8a (experiment 4) is not expected to resemble the real SST (and the GS path is probably a little too far north). Therefore, the focus here is on the changes in SST (relative to "No Hurricane" case, experiment 1) that were caused by surface winds (Fig. 8c; experiment 2), surface heat flux (Fig. 8; experiment 3) and both, winds + heat flux (Fig. 8b; experiment 4). A cooling of ~ 1–4 °C in SST is seen (Fig. 8b), but with very large spatial variations, including some warming on the onshore side of the GS front. The pattern of SST change for this hurricane is quite extensive and different than the typical cooling pattern seen in the wake of the path of other hurricanes (see for example, Fig. 3 in Bender and Ginis 2000, or Fig. 7 in Oey et al. 2007). The experiment with wind only (Fig. 8c) shows that these spatial variations are the result of the interaction of the wind with the GS—impact includes cooling along the warm core of the GS and (relative) warming of the onshore side of the GS and near the cold-core ring around 70°W, 38°N. In additional to the mixing effect of the wind, a slight northward shift of the GS front in the MAB (relative to the "no hurricane" case) can also cause this relative warming of the onshore side of the GS. The experiment with heat flux only (Fig. 8d) indicates a cooling trend everywhere, but especially large cooling on the shelf and the onshore side of the GS. It is expected that larger SST cooling will occur in regions with shallow continental shelves and shallow mixed layers, as documented in other studies (e.g., Oey et al. 2006, 2007).

To further look at the vertical extension of the impact, east-west cross sections of temperature across 38°N are shown in Fig. 9 (same experiments as in Fig. 8). The sea surface height (SSH) and stratification along this section (Fig. 9a) indicate that the section crosses the GS at ~ 73°W and crosses a cold-core ring at ~ 70–71°W. As shown in Fig. 8c, most of the spatial variations were due to the impact of the wind (Fig. 9c), which caused cooling of the continental shelf by upwelling and cooling of the upper ~ 50 m by vertical mixing.

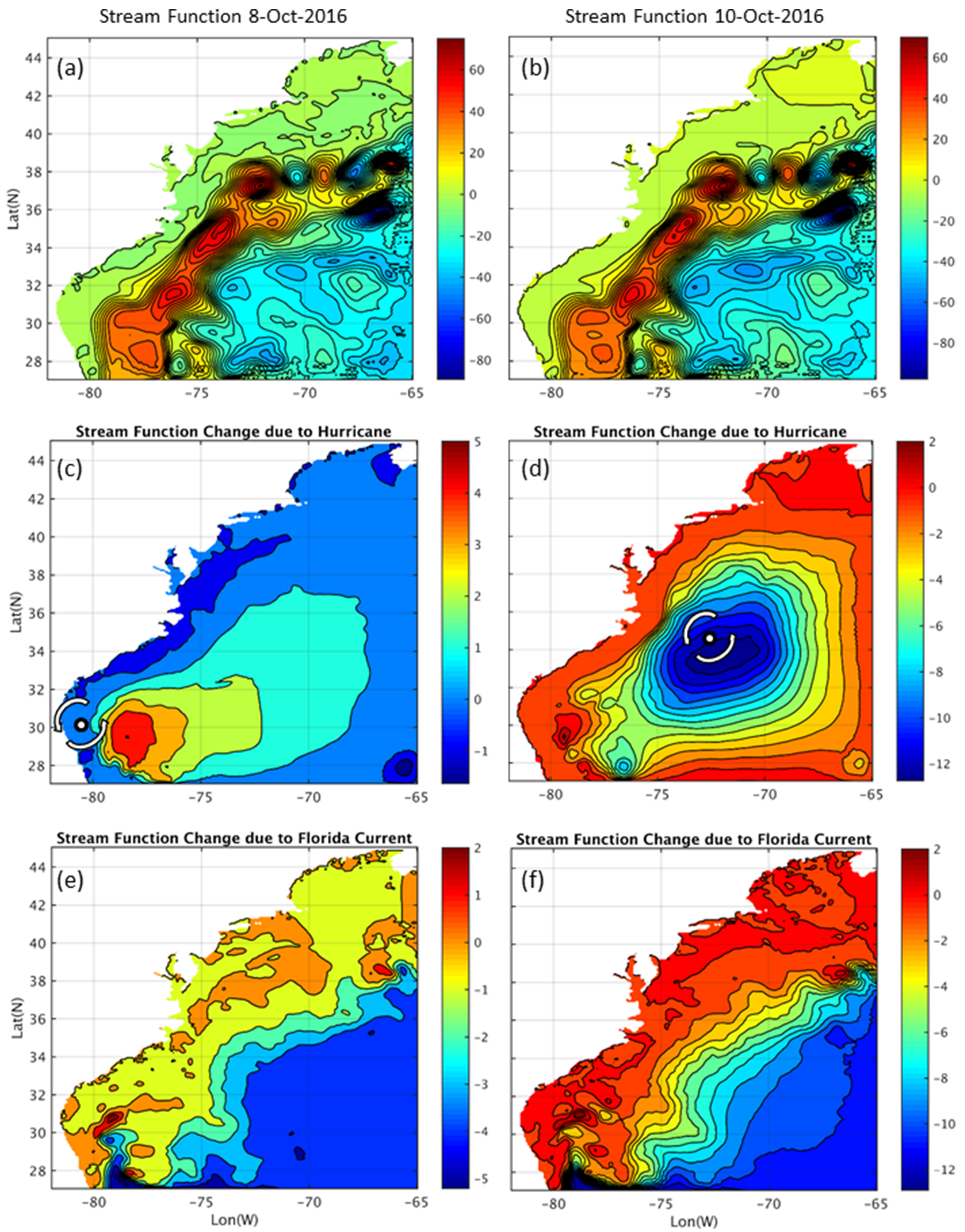

Fig. 7 Model stream function in Sv for **a** October 8 and **b** October 10, and the change at those dates due to the hurricane wind (**c**, **d**) and due to the FC (**e**, **f**). The change in transport is the difference between the simulation with and without hurricane (**c**, **d**; experiment 4 minus experiment 1) or with and without time-dependent FC (**e**, **f**; experiment 5 minus experiment 1). Note the different color bar scale in each panel, contour interval is 5 Sv in **a**–**b** and 1 Sv in **c**–**f**. The estimated location of the hurricane eye is indicated in **c**, **d**

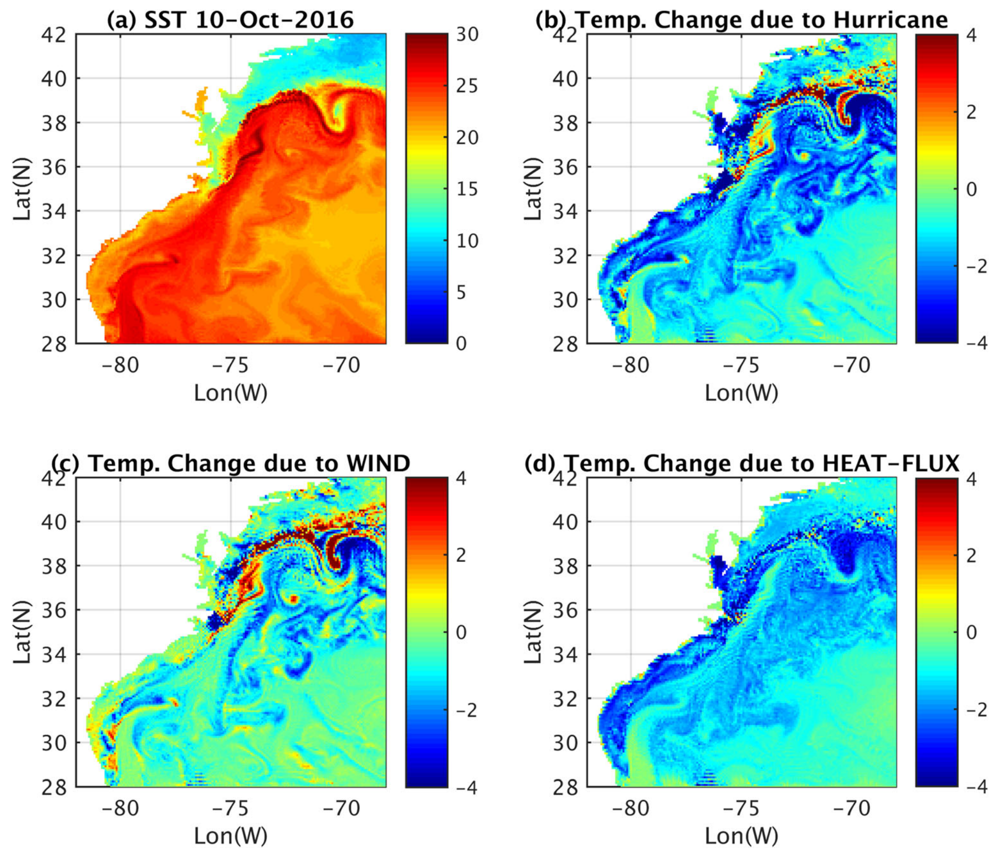

Fig. 8 **a** Model sea surface temperature (SST) on October 10 (experiment 4) and the impact of **b** WIND + HF (experiment 4 minus experiment 1), **c** WIND only (experiment 2 minus experiment 1), and **d** HF only (experiment 3 minus experiment 1

However, winds can also cause warming near the GS front and near the cold-core ring (mixing of the cold ring with surrounded warmer waters may have caused this). The impact of heat flux is more spatially even with a cooling trend

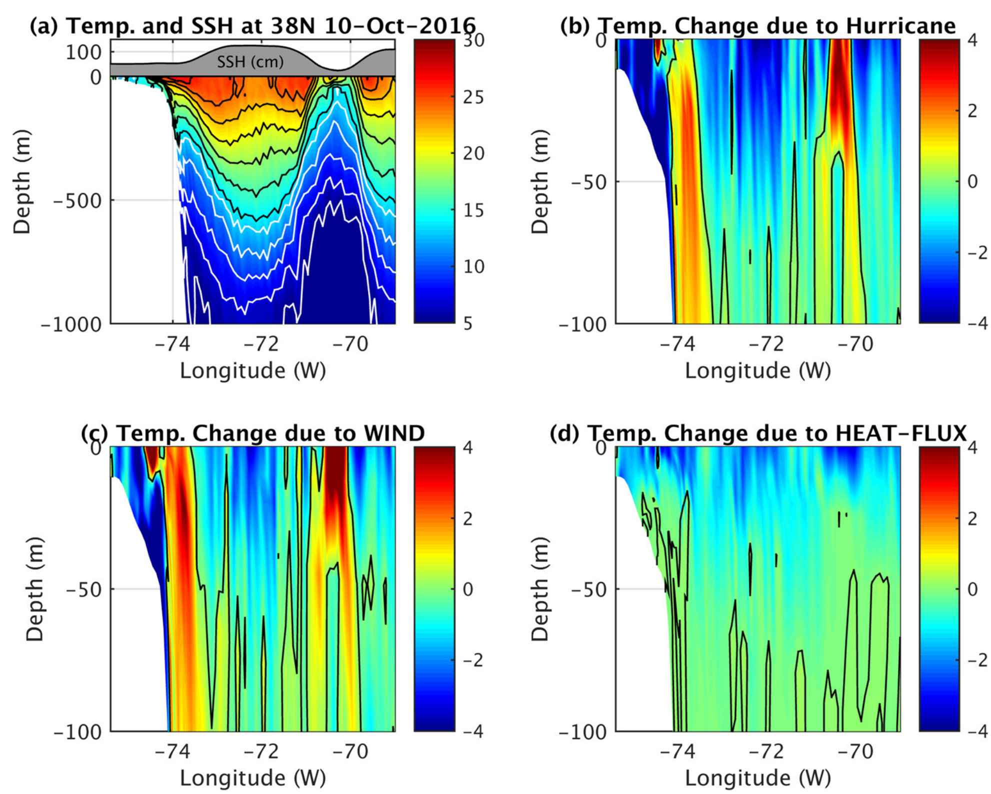

Fig. 9 East-west cross section at 38°N on October 10, 2016. **a** Temperature for hurricane case (experiment 4, WIND + HF), **b** temperature change due to the hurricane (experiment 4 minus experiment 1), **c** temperature change due to the WIND only (experiment 2 minus experiment 1), and **d** temperature change due to the HF only (experiment 3 minus experiment 1). Note that **b**–**d** only show the upper 100 m and the color bar is different than in **a**. Contour interval is 2°C in **a** and black contour in **b**–**d** is the zero line

everywhere above ~30 m (Fig. 8d). As shown by Oey et al. (2006), hurricanes can generate internal waves and very strong vertical velocities in their wake which may explain some of the variations in Fig. 9c. However, a more detailed study of these convective processes and breaking of internal waves will require the usage of non-hydrostatic models (e.g., Legg and Adcroft 2003), which is beyond the scope of this study.

3.4 The impact of the hurricane on kinetic and potential energy

To see how the hurricane impacted the upper ocean flow and the upper ocean stratification, the changes in mean kinetic energy and mean potential energy during the hurricane are estimated. The mean kinetic energy per unit mass of the upper 50 m averaged over the entire model domain is defined by

$$KE(t) = \frac{0.5}{VOL} \int_x \int_y \int_{z=-50m}^{0} \left[u(x,y,z,t)^2 + v\left(x,y,z,t\right)^2 \right] dxdydz \quad , \quad (4)$$

$$VOL = \int_x \int_y \int_{z=-50m}^{0} dxdydz$$

and the relative mean potential energy change per unit mass is defined here by

$$PE(t) = \frac{g}{VOL} \int_x \int_y \int_{z=-50m}^{0} z \left[\frac{\rho(x,y,z,t) - \rho_0(x,y,z)}{\rho_0(x,y,z)} \right] dxdydz \quad (5)$$

where the reference density ρ_o is the initial condition prior to the hurricane. In (5), cooling and increased density would result in more negative PE ($z < 0$), i.e., less energy is needed to mix the water column. One should not expect a balance between KE and PE in the upper 50 m, as input of wind energy involves momentum and heat exchange with deeper layers and the generation of eddy kinetic energy. The main purpose of these calculations is to evaluate the impact of the hurricane on the flow (4) and stratification (5). Therefore, the changes in upper ocean KE and PE are calculated as the difference of each case with the "no hurricane" (experiment 1), and the results are shown in Fig. 10. The maximum KE due to the hurricane winds (Fig. 10a) occurred on October 7. Note the slightly larger KE for "WIND only" (experiment 2) case compared with "WIND+HF" (experiment 4); the additional cooling in the WIND + HF case increases the density of the upper layers, thus reducing velocities since more energy is needed to move a layer with a larger mass. As expected, the impact of "HF" (experiment 3) or "FC" (experiment 5) alone on KE is much smaller than the wind impact. The reduction of the FC transport in the latter experiment seems to affect mostly the total transport (Fig. 7f) and much less so for the mean surface flow, except near the GS itself.

The change in PE is somewhat less expected, especially the "WIND" only case (green line in Fig. 10b) that indicates relative net warming of the upper layers despite the induced mixing. All the other cases indicate net cooling of the upper layers which increases density there and resulted in more negative PE. In the "WIND" only case, in addition to local warming spots near the GS front, most of the southeastern part of the model domain has warmed by advection of warm

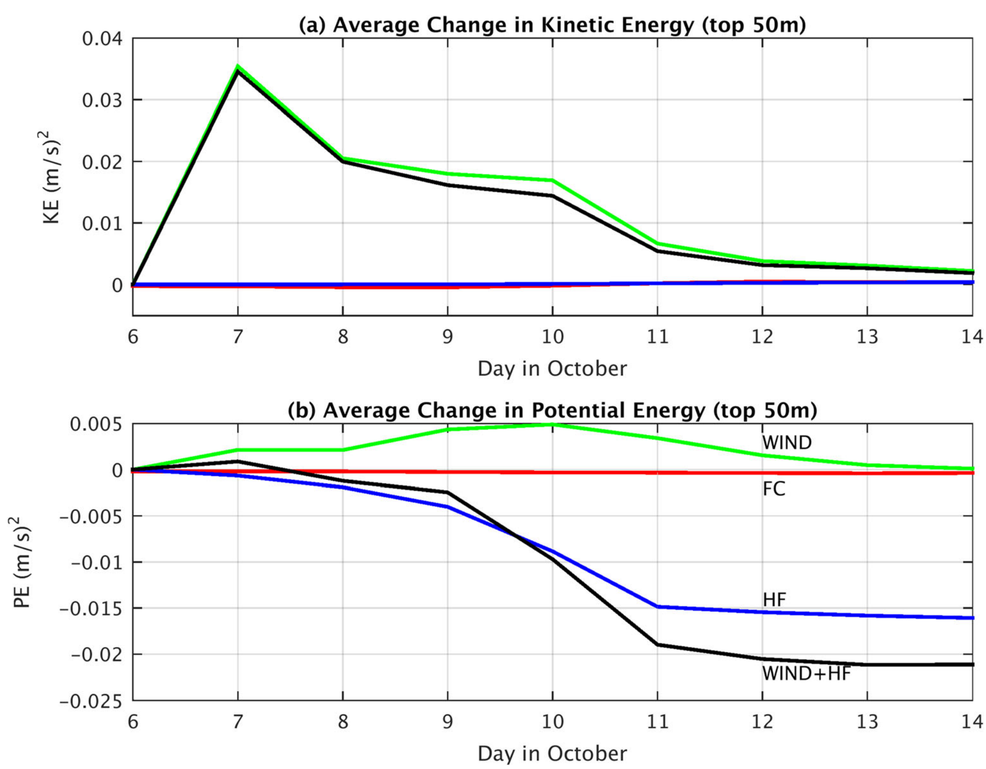

Fig. 10 Daily changes in the average **a** kinetic energy and **b** potential energy for the different experiments (in different color lines as indicated). The changes are the anomalies relative to the control run (no hurricane case). The values are energy per unit mass averaged over the upper 50 m of the entire model domain

waters from the south (Fig. 8c). This slight warming is explained by the fact that most of the model domain was under the influence of the northward winds east of the eye of the storm. The largest reduction in PE is for the “WIND+HF” case which induced more cooling than the separate impacts of “WIND” + “HF”. This result indicates the non-linear nature of the surface forcing where the maximum impact is obtained when wind-induced mixing is combined with surface heat loss. The impact of FC alone is a very small reduction in PE when the transport of the FC is reduced and the rate of warm waters advected from the Florida Strait downstream is reduced. One of the important conclusions from Fig. 10 is the difference in timing between the immediate KE increase by the hurricane winds (peak KE on October 7) and the delay response of PE that seems to last for days after the hurricane had dissipated. The disruption to the GS flow and erosion of the stratification can keep the GS in a state of weaker than normal flow (and elevated coastal water levels, as discussed before) for days after the hurricane disappeared. One can estimate how long it would take for the GS to completely recover by only advection of new warm waters from the Florida Strait downstream (neglecting wind and heat fluxes). At velocity speed of ~ 1 m s^{-1}, it would take warm waters from the Florida Strait almost a month to reach the northeastern part of the GS (~ 2500 km away). This can explain the unpredictable minor tidal flooding that are often observed following remote storms far away from the flooding area (Ezer and Atkinson 2014, 2016; Ezer et al. 2017).

4 Summary and conclusions

The interconnections between variations in the GS flow, variations in coastal sea level, and Atlantic Ocean variability over wide range of time scales have been an area of intense research in recent years. The long-term implications are related for example, to climate change and sea level rise acceleration due to potential GS slowdown (Sallenger et al. 2012; Ezer et al. 2013) while short-term variability is related for example, to increase in the frequency of minor tidal flooding (Ezer and Atkinson 2014), or the indirect effect of a hurricane on ocean dynamics (Ezer et al. 2017; Ezer 2018). Recent “clear-day” floods in coastal cities such as Norfolk, VA, often last several days after hurricanes passed off the Florida coast, even though the hurricanes remained thousands of kilometers away and never made landfall; examples are Hurricane Joaquin [2015] and Hurricane Matthew [2016]. A recent study of Hurricane Matthew (Ezer et al. 2017) used various observations and output from a coupled ocean-atmosphere operational forecast system to describe the disruption that the hurricane caused to the GS flow, which temporally weakened the GS and contributed to elevated coastal sea level (in addition to the storm surge). Following the above study, sensitivity experiments with a regional ocean model are conducted here to better understand the interplay between the hurricane, the GS and coastal sea level, using data from Hurricane Matthew.

The results demonstrate the distinctly different impact of surface heat loss versus surface wind stress versus the impact of the FC by comparing simulations with different forcing with simulations of the GS without the hurricane. Because of the passage of that hurricane near the strong currents of the GS, the pattern of SST change had much more spatial variations than usually seen in the wake of a hurricane (e.g., see Bender and Ginis 2000). The wind mixing and its interaction with the GS caused spatial changes to upper ocean temperatures near the GS front and near eddies (with local warming at some locations) while surface heat loss caused a more even cooling that is enhanced in shallow regions. The coastal sea level response to wind-driven storm surge is large near the storm, but that anomaly lasts for only a short period of few hours, while the response to disruption to the GS or related weakening of the FC seemed to last for days after the hurricane disappeared. Analysis of kinetic and potential energy confirms that it takes a long time for the stratification to recover after a hurricane—a week after the peak of the hurricane-induced kinetic energy, the potential energy remained low. This result can explain the observations that show elevated water levels and minor tidal flooding for days following a hurricane. Better understanding of these remote influences on coastal sea level can help to improve prediction models, which rely mostly on local wind, but have difficulty in accounting for indirect remote influence associated with ocean dynamics.

Acknowledgments Old Dominion University’s Climate Change and Sea Level Rise Initiative (CCSLRI) and the Resilience Collaborative (ODU-RC) provided partial support for this study and the Center for Coastal Physical Oceanography (CCPO) provided computational support. The hourly tide gauges sea level data are available from: (http://opendap.co-ops.nos.noaa.gov/dods/). The Florida Current transport record is obtained from: http://www.aoml.noaa.gov/phod/floridacurrent/. The HWRF model results are available from NOAA/NCEP (http://www.emc.ncep.noaa.gov/gc_wmb/vxt/HWRF/).

References

Baringer MO, Larsen JC (2001) Sixteen years of Florida current transport at 27°N. Geophys Res Lett 28(16):3,179–3,182. https://doi.org/10.1029/2001GL013246

Bender MA, Ginis I (2000) Real-case simulations of hurricane–ocean interaction using a high-resolution coupled model: effects on hurricane intensity. Mon Weather Rev 128:917–946. https://doi.org/10.1175/1520-0493(2000)128<0917:RCSOHO>2.0.CO;2

Blaha JP (1984) Fluctuations of monthly sea level as related to the intensity of the Gulf stream from key west to Norfolk. J Geophys Res Oceans 89(C5):8033–8042. https://doi.org/10.1029/JC089iC05p08033

Boon JD (2012) Evidence of sea level acceleration at U.S. and Canadian tide stations, Atlantic coast, North America. J Coast Res 28(6): 1437–1445. https://doi.org/10.2112/JCOASTRES-D-12-00102.1
Ezer T (2013) Sea level rise, spatially uneven and temporally unsteady: why the U.S. East Coast, the global tide gauge record, and the global altimeter data show different trends. Geophys Res Lett 40:5439–5444. https://doi.org/10.1002/2013GL057952
Ezer T (2015) Detecting changes in the transport of the Gulf stream and the Atlantic overturning circulation from coastal sea level data: the extreme decline in 2009-2010 and estimated variations for 1935-2012. Glob Planet Chang 129:23–36. https://doi.org/10.1016/j.gloplacha.2015.03.002
Ezer T (2016) Can the Gulf stream induce coherent short-term fluctuations in sea level along the U.S. East Coast?: a modeling study. Ocean Dyn 66(2):207–220. https://doi.org/10.1007/s10236-016-0928-0
Ezer T (2017) A modeling study of the role that bottom topography plays in gulf stream dynamics and in influencing the tilt of mean sea level along the U.S. East Coast Ocean Dyn 67(5):651–664. https://doi.org/10.1007/s10236-017-1052-5
Ezer T (2018) The increased risk of flooding in Hampton roads: on the roles of sea level rise, storm surges, hurricanes and the Gulf stream. In: the Hampton roads sea level rise preparedness and resilience intergovernmental pilot project, toll, R. And G. F. Kuska (Eds.). Mar Tech Soc J 52(2):34–44. https://doi.org/10.4031/MTSJ.52.2.6
Ezer T, Atkinson LP (2014) Accelerated flooding along the U.S. East Coast: on the impact of sea-level rise, tides, storms, the Gulf stream, and the North Atlantic oscillations. Earth's Future 2(8):362–382. https://doi.org/10.1002/2014EF000252
Ezer T, Atkinson LP (2017) On the predictability of high water level along the U.S. East Coast: can the Florida Current measurement be an indicator for flooding caused by remote forcing? Ocean Dyn 67(6):751–766. https://doi.org/10.1007/s10236-017-1057-0
Ezer T, Corlett WB (2012) Is sea level rise accelerating in the Chesapeake Bay? A demonstration of a novel new approach for analyzing sea level data. Geophys Res Lett 39:L19605. https://doi.org/10.1029/2012GL053435
Ezer T, Atkinson LP, Corlett WB, Blanco JL (2013) Gulf Stream's induced sea level rise and variability along the U.S. mid-Atlantic coast. J Geophys Res Oceans 118:685–697. https://doi.org/10.1002/jgrc.20091
Ezer T, Atkinson LP, Tuleya R (2017) Observations and operational model simulations reveal the impact of hurricane Matthew (2016) on the Gulf stream and coastal sea level. Dyn Atmos Oceans 80: 124–138. https://doi.org/10.1016/j.dynatmoce.2017.10.006
Garzon JL, Ferreira CM, Padilla-Hernandez R (2017) Evaluation of weather forecast system for storm surge modeling in the Chesapeake Bay. Ocean Dyn 68(1):91–107. https://doi.org/10.1007/s10236-017-1120-x
Goddard PB, Yin J, Griffies SM, Zhang S (2015) An extreme event of sea-level rise along the northeast coast of North America in 2009–2010. Nat Commun 6:6345. https://doi.org/10.1038/ncomms7346
Kourafalou VH, Androulidakis YS, Halliwell GR, Kang HS, Mehari MM, Le Hénaff M, Atlas R, Lumpkin R (2016) North Atlantic Ocean OSSE system development: nature run evaluation and application to hurricane interaction with the Gulf stream. Prog Oceanogr 148:1–25. https://doi.org/10.1016/j.pocean.2016.09.001
Legg S, Adcroft A (2003) Internal wave breaking at concave and convex continental slopes. J Phys Oceanogr 33(11):2224–2246. https://doi.org/10.1175/1520-0485(2003)033<2224:IWBACA>2.0.CO;2
Li Y, Xue H, Bane JM (2002) Air-sea interactions during the passage of a winter storm over the Gulf stream: a three-dimensional coupled atmosphere-ocean model study. J Geophys Res Oceans 107(C11). https://doi.org/10.1029/2001JC001161
Liu X, Wei J (2015) Understanding surface and subsurface temperature changes induced by tropical cyclones in the Kuroshio. Ocean Dyn 65(7):1017–1027. https://doi.org/10.1007/s10236-015-0851-9
McCarthy G, Frejka-Williams E, Johns WE, Baringer MO, Meinen CS, Bryden HL, Rayner D, Duchez A, Roberts C, Cunningham SA (2012) Observed interannual variability of the Atlantic meridional overturning circulation at 26.5°N. Geophys Res Lett 39(19): L19609. https://doi.org/10.1029/2012GL052933
Meinen CS, Baringer MO, Garcia RF (2010) Florida current transport variability: an analysis of annual and longer-period signals. Deep Sea Res 57(7):835–846. https://doi.org/10.1016/j.dsr.2010.04.001
Mellor GL, Hakkinen S, Ezer T, Patchen R (2002) A generalization of a sigma coordinate ocean model and an intercomparison of model vertical grids. In: Pinardi N and Woods JD (eds) Ocean forecasting: Conceptual basis and applications. Springer, Berlin, p 55-72. https://doi.org/10.1007/978-3-662-22648-3_4
Oey LY, Ezer T, Wang DP, Fan SJ, Yin XQ (2006) Loop current warming by hurricane Wilma. Geophys Res Lett 33:L08613. https://doi.org/10.1029/2006GL025873
Oey LY, Ezer T, Wang DP, Yin XQ, Fan SJ (2007) Hurricane-induced motions and interaction with ocean currents. Cont Shelf Res 27: 1249–1263. https://doi.org/10.1016/j.csr.2007.01.008
Park J, Sweet W (2015) Accelerated Sea level rise and Florida current transport. Ocean Sci 11:607–615. https://doi.org/10.5194/os-11-607-2015
Piecuch CG, Ponte RM (2015) Inverted barometer contributions to recent sea level changes along the northeast coast of North America. Geophys Res Lett 42:5918–5925. https://doi.org/10.1002/2015GL064580
Piecuch CG, Dangendorf S, Ponte R, Marcos M (2016) Annual sea level changes on the north American northeast coast: influence of local winds and barotropic motions. J Clim 29:4801–4816. https://doi.org/10.1175/JCLI-D-16-0048.1
Sallenger AH, Doran KS, Howd P (2012) Hotspot of accelerated sea-level rise on the Atlantic coast of North America. Nat Clim Chang 2:884–888. https://doi.org/10.1038/NCILMATE1597
Shay LK, Goni GJ, Black PG (2000) Effects of a warm oceanic feature on hurricane opal. Mon Weather Rev 128:1366–1383. https://doi.org/10.1175/1520-0493(2000)128<1366:EOAWOF>2.0.CO;2
Smeed DA, McCarthy G, Cunningham SA, Frajka-Williams E, Rayner D, Johns WE, Meinen CS, Baringer MO, Moat BI, Duchez A, Bryden HL (2013) Observed decline of the Atlantic meridional overturning circulation 2004 to 2012. Ocean Sci Discuss 10:1619–1645. https://doi.org/10.5194/osd-10-1619-2013
Tallapragada V, Bernardet L, Biswas MK, Gopalakrishnan S, Kwon Y, Liu Q, Marchok T, Sheinin D, Tong M, Trahan S, Tuleya R, Yablonsky R, Zhang X (2014) Hurricane Weather Research and Forecasting (HWRF) Model: 2014 Scientific documentation. In: Bernardet L (ed) NCAR development tested bed center report, 81pp, Boulder, CO
Wdowinski S, Bray R, Kirtman BP, Wu Z (2016) Increasing flooding hazard in coastal communities due to rising sea level: case study of Miami Beach, Florida. Ocean Coast Man 126:1–8. https://doi.org/10.1016/j.ocecoaman.2016.03.002
Woodworth PL, Maqueda MM, Gehrels WR, Roussenov VM, Williams RG, Hughes CW (2016) Variations in the difference between mean sea level measured either side of cape Hatteras and their relation to the North Atlantic oscillation. Clim Dyn 49(7–8):2451–2469. https://doi.org/10.1007/s00382-016-3464-1
Wu CR, Chang YL, Oey LY, Chang CWJ, Hsin YC (2008) Air-sea interaction between tropical cyclone Nari and Kuroshio. Geophys Res Lett 31:L12605. https://doi.org/10.1029/2008GL033942
Yablonsky RM, Ginis I, Thomas B, Tallapragada V, Sheinin D, Bernardet L (2015) Description and analysis of the ocean component of NOAA's operational hurricane weather research and forecasting (HWRF) model. J Atmos Ocean Technol 32:144–163. https://doi.org/10.1175/JTECH-D-14-00063.1